

# Cross-Modal Retrieval for Motion and Text via MildTriple Loss

Sheng Yan<sup>a</sup>, Haoqiang Wang<sup>a</sup>, Xin Du<sup>a</sup>, Mengyuan Liu<sup>b,\*</sup> and Hong Liu<sup>b</sup>

<sup>a</sup>School of Artificial Intelligence, Chongqing University of Technology

<sup>b</sup>Key Laboratory of Machine Perception, Shenzhen Graduate School, Peking University

## ARTICLE INFO

**Keywords:**

Cross-modal retrieval  
Motion-text retrieval  
Triplet loss  
Contrastive learning

## ABSTRACT

Cross-modal retrieval has become a prominent research topic in computer vision and natural language processing with advances made in image-text and video-text retrieval technologies. However, cross-modal retrieval between human motion sequences and text has not garnered sufficient attention despite the extensive application value it holds, such as aiding virtual reality applications in better understanding users' actions and language. This task presents several challenges, including joint modeling of the two modalities, demanding the understanding of person-centered information from text, and learning behavior features from 3D human motion sequences. Previous work on motion data modeling mainly relied on autoregressive feature extractors that may forget previous information, while we propose an innovative model that includes simple yet powerful transformer-based motion and text encoders, which can learn representations from the two different modalities and capture long-term dependencies. Furthermore, the overlap of the same atomic actions of different human motions can cause semantic conflicts, leading us to explore a new triplet loss function, MildTriple Loss. It leverages the similarity between samples in intra-modal space to guide soft-hard negative sample mining in the joint embedding space to train the triplet loss and reduce the violation caused by false negative samples. We evaluated our model and method on the latest HumanML3D and KIT Motion-Language datasets, achieving a 62.9% recall for motion retrieval and a 71.5% recall for text retrieval (based on R@10) on the HumanML3D dataset. Our code is available at <https://github.com/eanson023/rehamot>.

## 1. Introduction

The combination of natural language and images or videos has attracted wide attention [31, 35, 66, 24, 28], especially with impressive results from recent multimodal neural networks, such as CLIP [49] and DALL-E 2 [50]. Moreover, multimodal image-text retrieval [14, 67, 12] and video-text retrieval tasks [29, 27] have become research hotspots, but the problem of connecting 3D human motion sequences has yet to be explored on a large scale. The ability to automatically match natural language descriptions with accurate 3D human motion, i.e., 3D human pose sequences [37, 39, 65], will open the door to many applications, such as video surveillance [56, 38] and security applications that can search and identify specific events and behaviors through language descriptions and human motion [21]. Additionally, this technology can improve virtual reality applications, making them more intuitive by enabling them to better interpret users' movements and language. Furthermore, it could be applied in sports training and rehabilitation to retrieve specific motion sequences and rehabilitation plans, and to provide relevant guidance and recommendations through text descriptions.

Text-guided motion synthesis [46, 18, 54] has forged a bridge between human motion and natural language. TEMOS [46] introduces the Variational Autoencoder (VAE) architecture into this task, capable of generating different motion sequences based on textual descriptions. MDM [54] incorporated diffusion models into this task and proposed

a generative model based on an uncategorized diffusion to generate expressive and natural human actions. More relevant to our work, Delmas et al. [10] conducted bidirectional retrieval based on rich natural language and 3D human poses, providing a detailed annotation process for generating natural language synthesis descriptions from given 3D keypoints. However, the retrieval objects of their research are limited to static geometric human postures, which can be treated as a 3D volumetric image and are essentially within the scope of image-text retrieval.

We propose a novel model for cross-modal retrieval of 3D human motion sequences and texts, i.e., retrieving motion given a text query (motion retrieval) or retrieving text given a motion query (text retrieval). In this task, compared to retrieving static body poses, human motion sequences contain more information and higher dimensionality, making it a crucial challenge to establish an effective temporal modeling model for learning the representations of human motion and textual descriptions. Most previous work on modeling human motion data has used autoregressive feature extractors [36, 16, 45] that iterate to decode the next time frame given the past ones. However, these methods can produce drift over time, often losing the functionality they initially learned. In contrast, sequence-level feature extractors encode the entire sequence, allowing the interaction and integration of information at different positions in the sequence, thus effectively capturing the long-term dependency relationships in the sequence. Therefore, we adopted the powerful Transformer model [57], based on self-attention mechanism and proven effective in various sequence retrieval tasks [3]. We designed a simple yet powerful architecture that inputs both motion and text features into a

\*Corresponding author

 nkliuyifang@gmail.com (M. Liu)

ORCID(s): 0009-0003-6622-9705 (S. Yan); 0009-0006-8954-5331 (H. Wang); 0009-0003-6622-9705 (X. Du); 0000-0002-6332-8316 (M. Liu); 0009-0003-6622-9705 (H. Liu);

Transformer encoder before projecting them into the cross-modal joint space.

Then, a commonly used approach is to adopt contrastive learning to learn the similarity between motion-text pairs. This approach is based on defining positive and negative samples with respect to anchor and uses distance metric methods to associate data from different modalities within the same space. As such, a flexible principle is established: pulling anchor and positive samples together in the embedding space while pushing anchor away from multiple negative samples. This principle can be implemented in various ways, including max-margin loss [20], triplet loss [58, 59], and InfoNCE [68, 62]. In cross-modal retrieval tasks, positive samples are often defined as data from a heterogeneous modality with the same label as the anchor in the dataset, which have strong semantic associations with the anchor. Negative samples are randomly sampled from the entire distribution and have relatively weaker semantic associations with the anchor. For instance in motion retrieval, as shown in Figure 1, Positive (motion (i)) and Anchor (text (i)) have a strong semantic association, whereas randomly sampled motions (ii) and (iii) are the negative samples.

We use triplet loss to implement the contrastive learning principle. In image-text retrieval tasks, the triplet loss based on hard negative sample mining, Max of Hinges Loss (MH Loss), achieved breakthroughs [14, 40]. We extend this idea in our model. Since human motion can be understood as a combination of different atomic actions at multiple time steps, there often exist some common atomic actions between different motion sequences. Therefore, hard negative samples often have strong semantic associations, similar to positive sample, and can even better reflect the content of the anchor. As evidence in Figure 1, there is a strong similarity between Positive and Negative 1, and Anchor can also describe Negative 1. We refer to these hard negative samples as false negatives. Mining these false negatives with Conventional MH Loss may separate pairs that are actually strongly correlated, such as the motion-text pair (ii) (in blue). This approach is overly harsh and unreasonable.

The above-mentioned problem is another key challenge in this task. Removing false negative samples from the negative sample set can avoid unnecessary semantic conflicts caused by sampling these samples. We utilize intra-modal similarity, i.e., motion-to-motion similarity for the motion modality and text-to-text similarity for the textual modality, to guide the mining of soft-hard negatives for triplet loss training in the joint embedding space, thereby reducing the violation caused by false negatives. We refer to this soft-hard negative sample mining triplet loss approach as MildTriple Loss. As shown in Figure 1, Negative 2 is similar but not identical to Positive, and we refer to this negative sample as a soft-hard negative sample. Our MildTriple Loss selects to push it away to protect the semantic correlation of the blue pair instead of pushing away Negative 1. To evaluate the effectiveness of the method, we conducted detailed ablation studies on the latest HumanML3D [18] and KIT [47] motion-language datasets, and achieved favorable results.

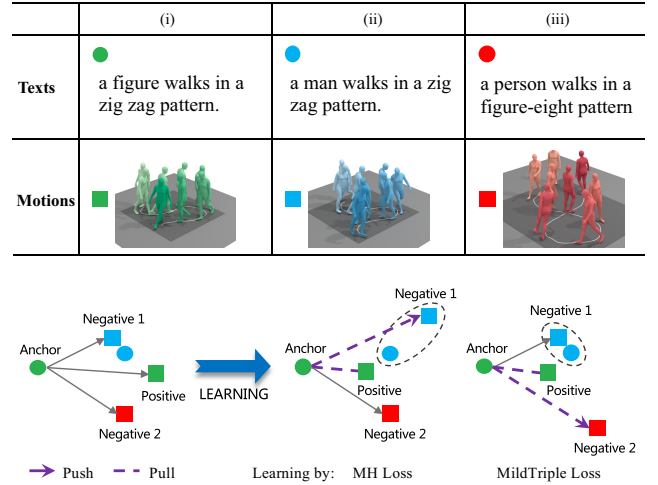


**Figure 1:** We show motion-text pairs from the HumanML3D dataset. Each image corresponds to a motion sequence, where the root trajectory of the body is projected onto the ground and the body posture is displayed at equidistant time frames. The flow of time is shown through color coding, where light colors represent the past. In the joint embedding space, the conventional MH Loss pushes Negative 1, which is closest to the anchor, thereby increasing the distance between the blue pair and creating a semantic conflict. In contrast, our MildTriple Loss pushes away the other negative sample, Negative 2, to maintain the semantic coherence of the blue pair.

Our main contributions can be summarized as follows:

- We contribute to the research by exploring the previously uncharted domain of cross-modal retrieval for 3D human motion sequences and text.
- We designed a model, which including Transformer-based motion and text encoders, to capture long-term dependencies for more accurate retrieval.
- To drive our model to learn more distinctive representations, we propose MildTriple Loss to address the unnecessary semantic conflicts caused by false negative samples.

The rest is organized as follows. In Section 2, we briefly discuss the related works. Our proposed methodology is described in Section 3. Experimental evaluation of the proposed methodology is presented, and the results and limitations are discussed in Section 4. Finally, in Section 5, we outline our conclusions and discuss our future works.

## 2. Related work

### 2.1. Motion-Text Embedding

Existing cross-modal retrieval methods mainly focus on text-based 2D [1] or 3D motion (sequence) synthesis [18, 54, 46]. One commonality with these methods is that they all construct joint cross-modal embeddings, mapping text and motion into the same space [46, 2, 61], which has been successful in other research fields [3, 22, 34]. When

modeling human motion, some methods use impoverished body motion representations. e.g., some do not model global trajectories [48, 61], and some do not model rotational information and linear velocity of joints [46, 2], resulting in unrealistic motion. In contrast, our work follows a more comprehensive motion representation method [18], which includes local joint positions, velocities, and 6D continuous rotation representations [69] in the root space. Furthermore, cross-modal representation learning models based on Transformers have become popular [15, 52, 43, 63]. VideoBERT [52] adopts the BERT design and applies it to quantize video representations, while VilBERT [43] combines BERT with joint learning of visual and language tasks, achieving joint learning of cross-modal representations of images and text and achieving excellent performance on multiple visual and language tasks. Some of the above work uses large-scale datasets to learn representations from scratch, while others compute input features from a given pre-trained expert model and learn joint embeddings. Our model combines both aspects and learns representations for motion and text respectively using the above approaches.

## 2.2. Sample Selection in Contrastive Learning

Recent works have proposed various sample selection methods in contrastive learning [22, 7, 55, 41, 9]. He et al. [22] introduced Momentum Contrast (MoCo) that constructs negative pairs using a dynamic dictionary of previously seen features. Chen et al. [6] proposed SimCLR, which uses data augmentation to form positive pairs and a large number of negative pairs. Other methods focus on selecting samples with high information content for contrastive learning. Tian et al. [55] proposed InfoMin, which uses mutual information to select informative samples for training. These methods belong to self-supervised learning, which learns the semantic relationship between images or text itself by pretext tasks on a large-scale dataset (millions of samples), and learn universal feature representations for various downstream tasks. Consequently, they require constructing a large number of negative pairs to improve the robustness and generalization ability of the model. In contrast, our research focuses on the matching task between motion and text, where pairwise similarity is sparser compared to that of contrastive images (or text) themselves. Hence, we use another negative sample selection method, namely, hard negative mining, which has been shown to work well in contrastive learning [14, 40, 67, 71, 4]. Furthermore, our sample selection is influenced by the IMC loss proposed by Chen et al. [5] which optimizes the intra-modal space by constraining the violation of negative pairs within the same homogeneous modality using a threshold. We also use the idea of threshold control, but we do not optimize the intra-modal space. Additionally, our concept of false negative samples resembles the influential sample concept proposed in CrossCLR [70], but with a different definition. Specifically, CrossCLR defines influential samples as samples with high connectivity to other samples, while our false negative samples are defined

as negative samples with high similarity to positive samples or mapping samples with high similarity to anchor.

## 3. Method

### 3.1. Task Definition

**Text descriptions** represent the description of human motion in written natural language sentences, such as in English. The sentence contains an accurate sequence of actions, such as "*a person holds their arms out, lowers them, then walks forward and sits down*" or "*hands in air doing a climbing upward motion*." The data structure is a word sequence  $\mathbf{t} = (w_1, \dots, w_N)$ ,  $w \in \mathbb{R}^{D_w}$  of length  $N$  (with each word counted as 1) from the English vocabulary, where  $D_w$  represents the word embedding dimension.

**3D human motion** is defined as a series of human poses  $\mathbf{m} = (f_1, \dots, f_F)$ ,  $f \in \mathbb{R}^{D_p}$ , where  $F$  represents the number of time frames. Each posture  $f$  corresponds to the representation of an articulated human body. In this article, we use joint rotations, joint positions, and foot contact conditions to represent the body motion of each posture  $f$ , forming a  $D_p$ -dimensional feature vector. A more detailed definition will be given in Section 4.1.

**Task objective.** For motion retrieval, given a query in text, the task is to retrieve the most relevant human motion sequences from a database. Similarly, for text retrieval, the query is a human motion, and the task is to retrieve relevant text. The objective is to maximize recall at  $K$  ( $R@K$ ), where the fraction of queries ranked among the top  $K$  items returned is the most relevant [25] ( $K$  is typically 1-10). Let  $\mathcal{D} = \{(m_i, t_i)\}_{i=1}^I$  be the training set of motion-text pairs. We call  $(m_i, t_i)$  a positive pair, and  $(m_i, t_{j \neq i})$  a negative pair. Thus, we have  $I$  positive pairs and  $I^2 - I$  negative pairs in the training set. To achieve satisfactory performance at  $R@K$ , we need to maximize the similarity of  $I$  positive pairs in the training set, while minimizing the similarity of  $I^2 - I$  negative pairs.

### 3.2. Model Architecture

We use a dual-branch network to extract motion and text features, and project heterogeneous modal features into a joint embedding space, whereby we learn representations via the MildTriple loss. As depicted in Figure 2, a typical "paired embedding learning" architecture is adopted. We parameterize the motion and text encoders prior to the projection layer as  $\mathcal{M}_{enc}(\cdot; \theta_\phi)$  and  $\mathcal{T}_{enc}(\cdot; \theta_\psi)$ , respectively. For the motion encoder, the encoder can take arbitrary-length pose sequences as input and output motion features, denoted as  $\mathcal{T}_m$ . Before feeding each human body pose into the transformer encoder, we embed it into a  $D_\ell$ -dimensional space at the embedding layer. As we embed any arbitrary-length sequence into a latent space (sequence-level embedding), we need to pool the temporal dimension. In other fields, a [cls] token has been introduced for pooling, such as ViT [13] in computer vision and more early BERT [11] in NLP. Inspired by this approach, we add a learnable token  $\mathcal{T}_m$  before the input and only use the corresponding encoder

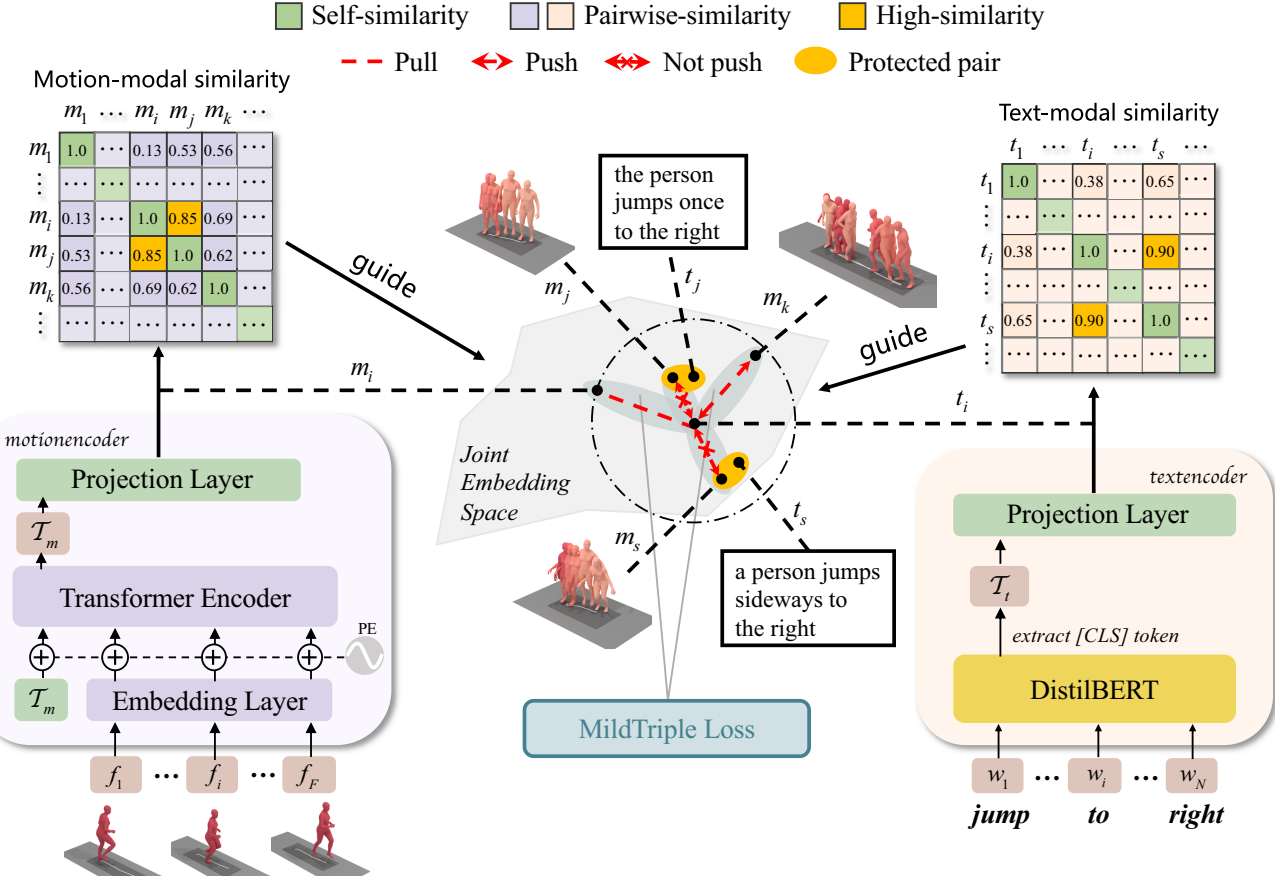


**Figure 2:** Our proposed framework encodes motion and text separately by inputting them into their respective encoders. Specifically, in the motion branch, a learnable token  $T_m$  is inputted along with the embedded pose sequence into a Transformer encoder, and the motion feature output is extracted. In the text branch, the [cls] token  $T_t$  is extracted from the pre-trained and frozen DistilBERT model[51], and used as the text feature output. Finally, the feature output is projected and mapped to a joint embedding space. In the same training batch, the MildTriple Loss encourages the motion embedding  $m_i$  and its textual embedding  $t_i$  to be close in this space. Simultaneously, through the guidance of similarity within each modality, (1) it prevents pushing away the motion embedding  $m_j$  that has high similarity with  $m_i$ , and (2) it avoids pushing away the motion embedding  $m_s$  whose text embedding  $t_s$  has high similarity with  $t_i$ . Instead, the MildTriple Loss guides the separation of another motion embedding  $m_k$  to preserve the semantic correlation of the yellow pairs.

output as a way to pool the temporal dimension. To do so, we append the embedded pose sequence to the token. The resulting transformer encoder input is the sum of position encoding given in the form of sinusoidal functions. By extracting the first output of the transformer encoder that corresponds to the token (i.e., discarding the rest), we obtain the motion feature output  $T_m$ . For the text encoder, we use the pre-trained expert model DistilBERT [11] as the backbone network and extract the  $D_w$ -dimensional [cls] token  $T_t$  as the text feature output. We freeze the weights of DistilBERT unless stated otherwise.

Next, we utilize linear projections  $h(\cdot; W_h)$  and  $g(\cdot; W_g)$  to define feature embeddings mapped to a joint embedding space. We also define a similarity function  $S(\cdot, \cdot)$  to measure the similarity between them. Mathematically, the entire

process can be formulated as:

$$\begin{aligned} S(m, t) &= h(T_m; W_h) \cdot g(T_t; W_g) \\ T_m &= f_{\text{extract}}(\mathcal{M}_{\text{enc}}(m; \theta_\phi)), T_m \in \mathbb{R}^{D_\ell} \\ T_t &= f_{\text{extract}}(\mathcal{T}_{\text{enc}}(t; \theta_\psi)), T_t \in \mathbb{R}^{D_w} \end{aligned} \quad (1)$$

where  $\cdot$  denotes inner product,  $W_h \in \mathbb{R}^{D_\ell \times D}$  and  $W_g \in \mathbb{R}^{D_w \times D}$ . The relevant encoder feature outputs  $\mathcal{T}$  is represented by selecting the first vector from the output sequence of either  $\mathcal{M}_{\text{enc}}(\cdot; \theta_\phi)$  or  $\mathcal{T}_{\text{enc}}(\cdot; \theta_\psi)$ , using the function  $f_{\text{extract}}$ . Prior to computing the inner product, we apply  $\ell_2$ -normalization to feature embeddings. In this case, the inner product is equivalent to cosine similarity [8]. Letting  $\theta = \{W_h, W_g, \theta_\phi\}$  be the overall model parameters, and if we also need to fine-tune the  $\mathcal{T}_{\text{enc}}$  network, then  $\theta$  will also be included in  $\theta_\psi$ .

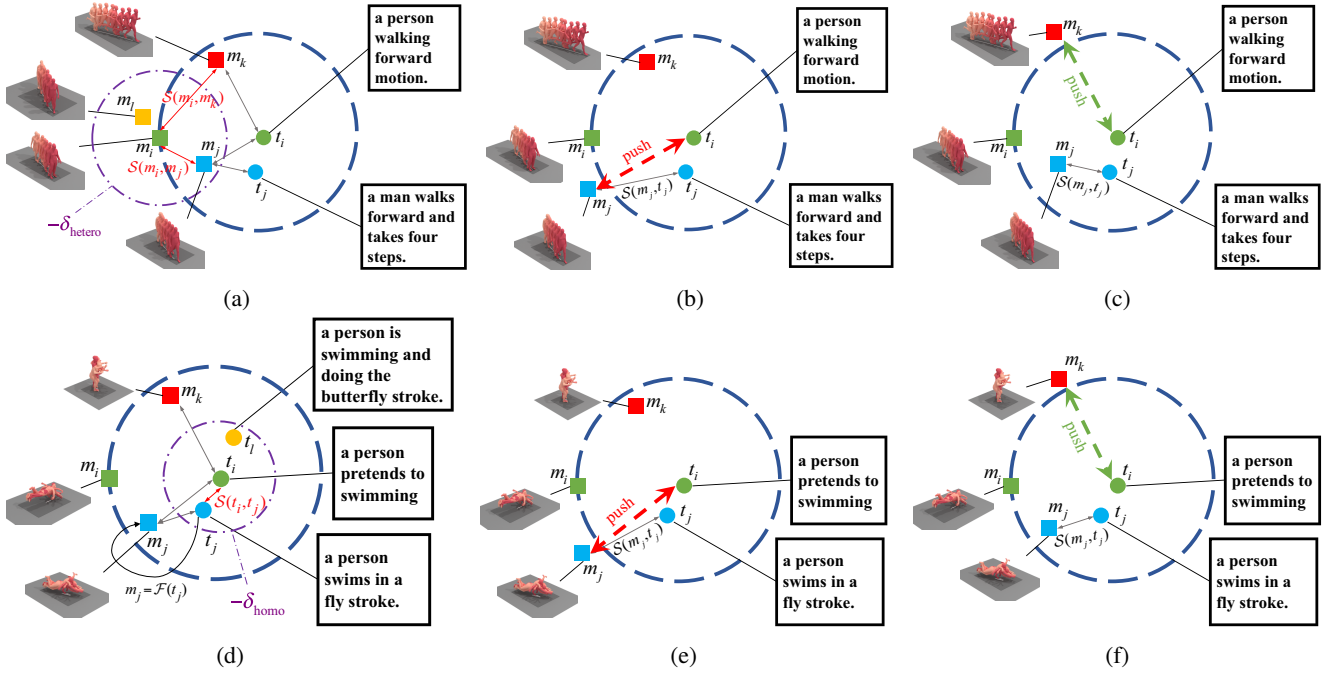


**Figure 3:** In the joint embedding space,  $t_i$  is the anchor and  $m_i$  is its positive sample, and the other squares and solid circles in sub-figures represent  $t_i$ 's heterogeneous negative samples and homogeneous negative samples, respectively. Here, we assume the similarity score to be negative distance, with a zero margin  $\alpha$ . In sub-figure 3a, we consider heterogeneous negative samples whose similarity score with the positive  $m_i$  is greater than  $\delta_{\text{hetero}}$  as false negatives, e.g.,  $m_j$  and  $m_l$ , both representing walk forward motion like  $m_i$ . Meanwhile, if a sample has a similarity score less than  $\delta_{\text{hetero}}$  and is the closest among heterogeneous negatives to anchor  $t_i$ , it is identified as a soft-hard negative sample. e.g.,  $m_k$ , which represents forward running, is semantically similar but different from  $t_i$ . During training, the MH Loss encourages the false negative  $m_j$  that is closest to  $t_i$  (i.e., has the highest similarity) to move away, as shown in sub-figure 3b. This decreases the similarity score  $S(m_j, t_i)$  for the positive pair  $(m_j, t_i)$ , eventually leading to semantic conflicts. In contrast, our MildTriple Loss abandons pushing away  $m_j$ , instead pushing away the soft-hard negative  $m_k$  to protect the semantic relevance of the positive pair  $(m_j, t_i)$ , as shown in sub-figure 3c. This ensures that similarity score  $S(m_j, t_i)$  remains unchanged. Additionally, for the homogeneous negative samples whose similarity score with the anchor  $t_i$  is greater than  $\delta_{\text{homo}}$ , we consider their corresponding mapping samples to also be false negatives. e.g., the text  $t_j$  that describes swimming like  $t_i$ , has a mapping sample  $m_j$ , which we also consider to be a false negative. Hence, during training, the negative sample mining strategies of MH Loss and MildTriple Loss produce the same results as in sub-figures 3e and 3f, respectively.

### 3.3. Learning Objective

**Triplet Ranking Loss** (also known as Sum of Hinges Loss in [14], hereafter referred to as SH Loss), has been widely used in other cross-modal retrieval tasks, such as [33, 67, 60]. We employ it to compare with MildTriple loss and support its warm-up. After embedding the feature of motion and text into a common space, this ranking-based triplet loss is utilized to maximize the similarity of  $I$  positive pairs and minimize the similarity of  $I^2 - I$  negative pairs. We apply this approach to learn the model parameters  $\theta$  and minimize the cumulative loss of the training data  $\mathcal{D} = \{(m_i, t_i)\}_{i=1}^I$ , given by:

$$\begin{aligned} \mathcal{L}_{\text{SH}}(\theta, \mathcal{D}) = & \sum_{i=1}^I \sum_{\hat{t} \in \mathcal{Q}_T} [\alpha + \mathcal{d}(m_i, t_i) - \mathcal{d}(m_i, \hat{t})]_+ \\ & + \sum_{i=1}^I \sum_{\hat{m} \in \mathcal{Q}_M} [\alpha + \mathcal{d}(m_i, t_i) - \mathcal{d}(\hat{m}, t_i)]_+ \end{aligned} \quad (2)$$

where  $\alpha$  is a margin hyperparameter, and  $[x]_+ \equiv \max(0, x)$ .  $\mathcal{Q}_M = \{m_j \mid j \in [I] \setminus \{i\}\}$  and  $\mathcal{Q}_T = \{t_j \mid j \in [I] \setminus \{i\}\}$

represent the sets of negative samples for motion and text, respectively. The function  $\mathcal{d}(x, y)$  is the distance function between two vectors  $x$  and  $y$ . If the distance between  $m$  and  $t$  is closer to a given margin value  $\alpha$  than any negative sample, then the triplet loss is zero. In this paper, we use cosine distance [5] as the distance metric, expressed as  $\mathcal{d}(x, y) = 1 - S(x, y)$ , where  $S(x, y)$  is the cosine similarity mentioned above. The accumulated loss can be derived further as:

$$\begin{aligned} \mathcal{L}_{\text{SH}}(\theta, \mathcal{D}) = & \sum_{i=1}^I \sum_{\hat{t} \in \mathcal{Q}_T} [\alpha - S(m_i, t_i) + S(m_i, \hat{t})]_+ \\ & + \sum_{i=1}^I \sum_{\hat{m} \in \mathcal{Q}_M} [\alpha - S(m_i, t_i) + S(\hat{m}, t_i)]_+ \end{aligned} \quad (3)$$

**False Negative Sample Definition.** False negative samples actually have strong semantic overlap with positive samples, such as “a person walking forward motion.” and “a man walks forward and takes four steps.”. By contrasting these unwanted false negative pairs, the network is encouraged to discard their common features in the learned embeddings,

which goes against the common assumption in contrastive learning that having enough negative samples helps to learn better representations (e.g., [22, 64, 41]), because the model contrasts more semantic representations in each training batch. Therefore, when the number of false negative samples is large, frequent semantic conflicts [70] can hinder the algorithm from learning good representations.

To reduce the impact of semantic conflicts, we need to exclude these false negative samples from the negative sample set. For simplicity, we only describe the definition of the false negative sample set  $\mathcal{Y}_M$  using motion retrieval. For any positive pair  $(m, t)$  in dataset  $\mathcal{D}$ , where there exists a mapping relationship  $m = \mathcal{F}(t)$ ,  $m$  is referred to as the mapping sample of  $t$ . Consequently, the negative sample set  $\mathcal{Q}_M$  can be obtained by mapping  $\mathcal{Q}_T$ , such that  $\mathcal{Q}_M = \{\mathcal{F}(t_j) \mid \forall t_j \in \mathcal{Q}_T\}$ . Given the anchor text query  $t_i$  and its corresponding positive sample motion  $m_i$ . We extend the concept of negative samples in contrastive learning to two modalities, as shown in Figure 3a. Specifically, the elements in the original negative sample set  $\mathcal{Q}_M$  are referred to as heterogeneous negative samples (i.e., in a different modality than the anchor  $t_i$ ) and the elements in  $\mathcal{Q}_T$  as homogeneous negative samples (i.e., in the same modality as the anchor  $t_i$ ). We define false negative samples as those heterogeneous negative samples that are highly similar to the positive sample  $m_i$ . Moreover, we also consider the mapping sample of a homogeneous negative sample that is highly similar to the anchor  $t_i$  to be false negatives, as we believe that if a homogeneous negative sample is similar to  $t_i$ , then its corresponding mapping sample must have strong semantic relevance to  $m_i$ . We can control the threshold to determine the degree of similarity of samples that can be defined as false negative samples, as shown in Figure 3. Thus, the false negative sample-containing set  $\mathcal{Y}_M$  can be expressed as:

$$\begin{aligned} \mathcal{Y}_M = \{m_j \mid S(m_i, m_j) > \delta_{hetero}, \forall m_j \in \mathcal{Q}_M\} \\ \cup \{\mathcal{F}(t_j) \mid S(t_i, t_j) > \delta_{homo}, \forall t_j \in \mathcal{Q}_T\} \end{aligned} \quad (4)$$

where  $\delta_{hetero}$  and  $\delta_{homo}$  represent the thresholds for heterogeneous and homogeneous samples, respectively. When the similarity is greater than the threshold, the sample (mapping sample) is defined as a false negative sample. Similarly, the false negative sample set  $\mathcal{Y}_T$  for text retrieval can be derived in the same way:

$$\begin{aligned} \mathcal{Y}_T = \{t_j \mid S(t_i, t_j) > \delta_{hetero}, \forall t_j \in \mathcal{Q}_T\} \\ \cup \{\mathcal{F}(m_j) \mid S(m_i, m_j) > \delta_{homo}, \forall m_j \in \mathcal{Q}_M\} \end{aligned} \quad (5)$$

**MildTriple Loss.** Faghri et al. [14] demonstrated that the SH Loss 3 can lead to local minima when multiple negatives with small violations dominate the loss. To tackle this issue, they proposed the Max of Hinges (MH) Loss that employs hard negative sample mining. Recent studies [40, 67] have showed that the triplet loss based on hard negative sample mining achieves excellent performance in cross-modal retrieval tasks. Building upon this, our method extends the approach. To reduce the impact of false negative samples in contrastive learning, we decided to remove all false negative

samples (in each modality) from the negative sample set. Therefore, we redefine the negative sets for text retrieval and motion retrieval as:  $\hat{\mathcal{N}}_T = \{t_k \mid \forall t_k \in \mathcal{Q}_T, t_k \notin \mathcal{Y}_T\}$  and  $\hat{\mathcal{N}}_M = \{m_k \mid \forall m_k \in \mathcal{Q}_M, m_k \notin \mathcal{Y}_M\}$ . This negative set pruning strategy makes it easy to guide the model to mine soft-hard negative samples during the training. Hence, the objective function to minimize is as follows:

$$\begin{aligned} \mathcal{L}_{mild}(\theta, \mathcal{D}) = \sum_{i=1}^I [\alpha - S(m_i, t_i) + S(m_i, t')]_+ \\ + \sum_{i=1}^I [\alpha - S(m_i, t_i) + S(m', t_i)]_+ \end{aligned} \quad (6)$$

where  $t' = \text{argmax}_{t_j \in \hat{\mathcal{N}}_T} S(m_i, t_j)$  and  $m' = \text{argmax}_{m_j \in \hat{\mathcal{N}}_M} S(m_j, t_i)$  represent the hardest negative samples in their respective pruned negative sets. In our view,  $t'$  and  $m'$  are soft-hard negative samples that may have only slight correlations with the query and are not necessarily semantically consistent with it. Optimizing on these samples can help to avoid local minima. On the other hand, if  $t' = \text{argmax}_{t_j \in \mathcal{Q}_T} S(m_i, t_j)$  and  $m' = \text{argmax}_{m_j \in \mathcal{Q}_M} S(m_j, t_i)$ , then it represents the MH Loss in previous work. Figure 3 further explains the negative sample mining strategy of the two losses and compares the adaptivity of the two losses in motion-text retrieval task. To achieve computational efficiency, we select these negatives from each mini-batch rather than the entire training set.

## 4. Experiments

### 4.1. Datasets, Pose Representation and Metrics

**Datasets.** We conducted experiments and evaluations on two datasets, HumanML3D [18] and KIT-ML [47]. HumanML3D is a recent dataset that was re-annotated in text form from the AMASS [44] and HumanAct12 [19] collections of motion capture data. It contains 14,616 motions annotated with 44,970 textual descriptions, with an average of 3 relevant descriptions per action. Some descriptions only cover parts of certain actions due to their complexity, we consider these sub-actions and corresponding textual descriptions as additional ground-truth pairs. Thus, the dataset contains 15,541 motions. We used the downsampled data to 20 fps and split the dataset into a training set with 14,541 motions and a test set with 1,000 motions. KIT-ML dataset is composed of subsets of the KIT WholeBody Human Motion Database and the CMU Graphics Lab Motion Capture Database. It contains 3,911 motions and 6,353 sequence-level descriptions, with an average of 9.5 words per description. Among them, 3,008 sequences are valid with textual annotations, and each action has 1-8 relevant descriptions, totaling 6,349 textual descriptions. We used the downsampled data to 12.5 fps and split the dataset into a training set with 2,508 motions and a test set with 500 motions.

**Pose Representation.** We adopt the redundant pose representation provided in [18]. A pose  $f$  is defined by the

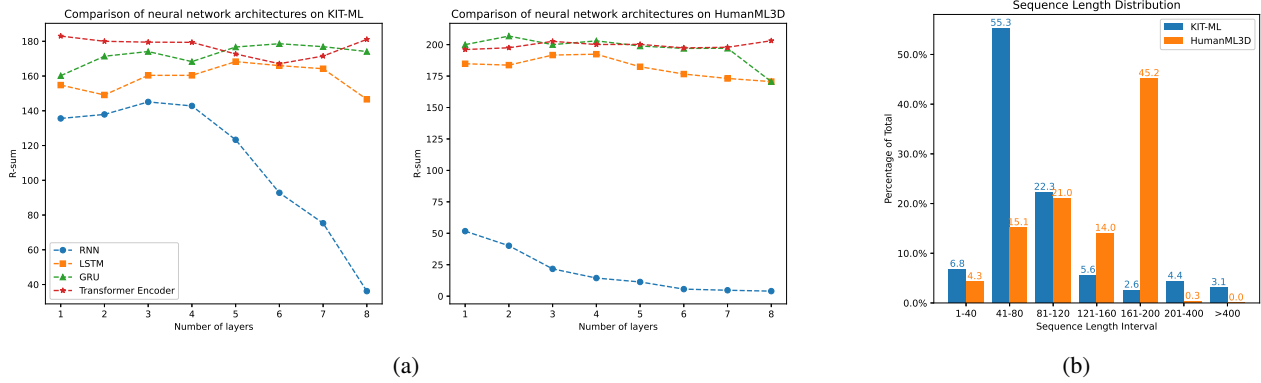


**Figure 4:** Sub-figure 4a presents a comparison of different neural network architectures and layers, displaying the results of contrast experiments conducted on the KIT-ML dataset on the left, and the HumanML3D dataset on the right. Sub-figure 4b shows the distribution of motion sequence lengths in both datasets.

tuple  $(\dot{r}^a, \dot{r}^x, \dot{r}^z, \dot{r}^y, \mathbf{j}^p, \mathbf{j}^v, \mathbf{j}^r, \mathbf{c}^f)$ , where  $\dot{r}^a \in \mathbb{R}$  is the root angular velocity along the Y-axis;  $(\dot{r}^x, \dot{r}^z) \in \mathbb{R}$  are the root linear velocities in the XZ plane;  $\dot{r}^y \in \mathbb{R}$  is the root height;  $\mathbf{j}^p \in \mathbb{R}^{3j}$ ,  $\mathbf{j}^v \in \mathbb{R}^{3j}$  and  $\mathbf{j}^r \in \mathbb{R}^{6j}$  are the local joint rotation-invariant position [26], velocity, and 6D continuous rotation [69] in the root space, where  $j$  is the number of joints; and  $\mathbf{c}^f \in \mathbb{R}^4$  is a binary feature obtained by thresholding the velocities of the heel and toe joints to emphasize foot-ground contact. The motion of the HumanML3D dataset follows the skeleton structure of 22 joints in SMPL [42], and each motion sequence is represented as  $\mathbf{m} \in \mathbb{R}^{F \times 263}$ . For the KIT-ML dataset, the poses have 21 joints, and  $\mathbf{m} \in \mathbb{R}^{F \times 251}$ . All human motion sequences are initially facing the Z+ direction.

**Evaluation Metrics.** We evaluated the learned embeddings for cross-modal retrieval tasks based on several metrics, including Recall@K (R@K), Median Rank (Med R), and R-sum [25, 17]. Given a query, we retrieve the K=[1, 5, 10] nearest neighbors from the database. Retrieval is considered successful if the correct sample is among the K nearest neighbors. R-sum is defined as follows:

$$R - \text{sum} = \overbrace{R@1 + R@5 + R@10}^{\text{Motion Retrieval}} + \overbrace{R@1 + R@5 + R@10}^{\text{Text Retrieval}} \quad (7)$$

## 4.2. Training Strategy

For all experiments listed in sections 4.3, 4.4 and 4.5, we used the AdamW optimizer [32] with a learning rate of 0.0002 for 60 epochs and set the joint embedding space  $D$  to 1024 with a margin  $\alpha$  of 0.2. For the motion branch, the dimension of the backbone network,  $D_l$ , was set to 256 to match the embedding layer. For the text branch, DistilBERT [51] was used to generate 768-dimensional feature output with  $D_j$  being set to 768. Due to limited computing resources, we abandoned training and testing data for motion sequences longer than 1000 frames (after downsampling), and set the batch size to 32 for KIT-ML and 64 for HumanML3D. In the contrast experiment 4.3, we replaced the

transformer encoder with other mainstream neural network models and used SH loss as the loss function. We chose the network with exceptional performance to be the backbone of the motion branch and used it for subsequent experiments, i.e., 1-layer transformer encoder for KIT-ML and 3-layer for HumanML3D. In the ablation study 4.4, we adopted the training strategy suggested in [14] of warming up the entire model for 5 epochs using SH loss to accelerate training. The thresholds  $\delta_{\text{hetero}}$  and  $\delta_{\text{homo}}$  were empirically set to 0.6 and 0.9 for KIT-ML, 0.7 and 0.9 for HumanML3D. To achieve better performance, we reduced the learning rate by ten times at the 30th epoch. Specifically, for the case where the training of the model using MH Loss on HumanML3D starts slowly, we extended the learning rate decay at the 45th epoch and continued training for another 30 epochs after training ended. Finally, when fine-tuning the language model parameters, we used a learning rate of 0.0002 for the text branch backbone network (i.e., DistilBERT) while keeping the learning rate constant for the remaining networks, and trained an additional 30 epochs.

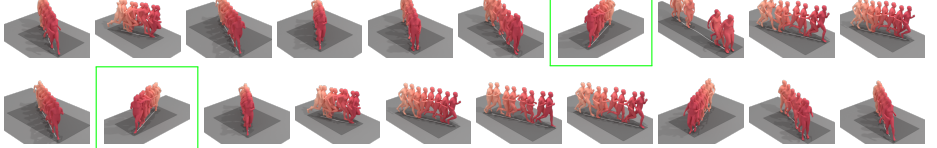
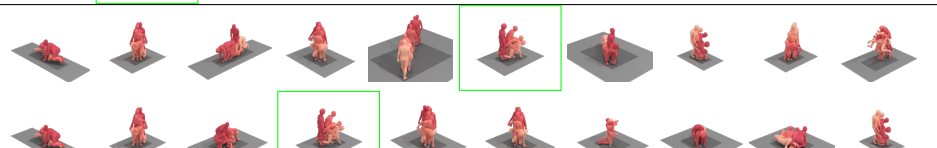
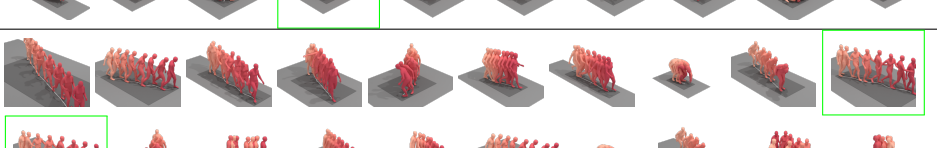
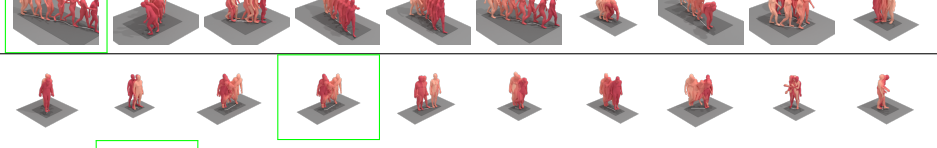
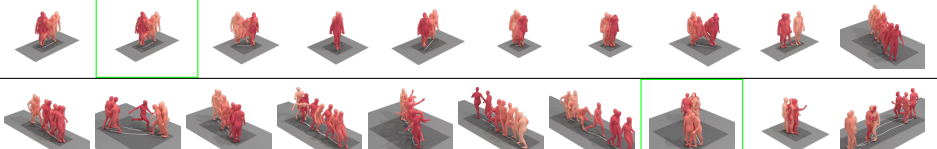
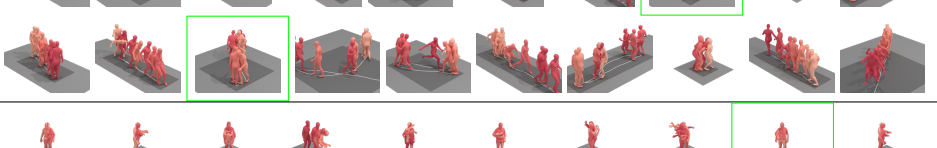
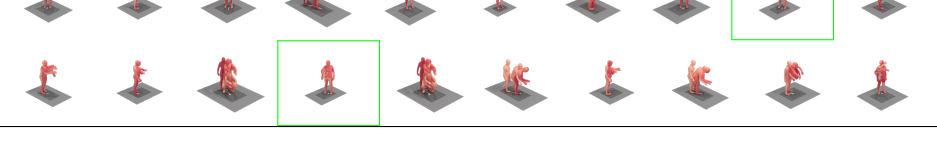
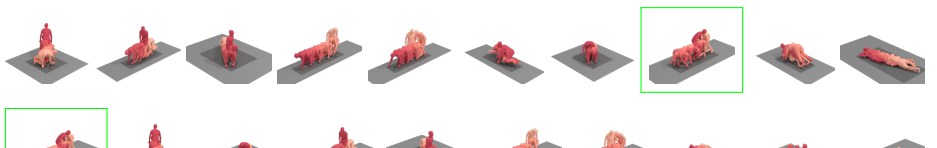
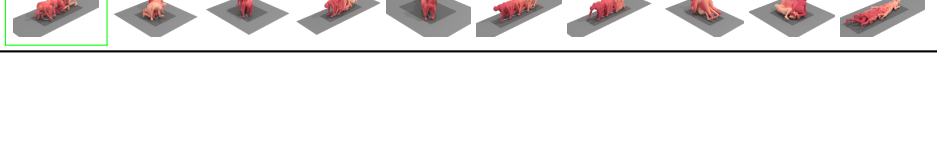
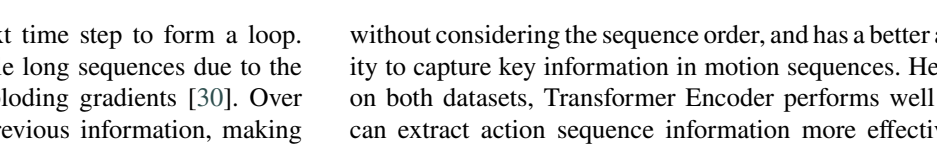
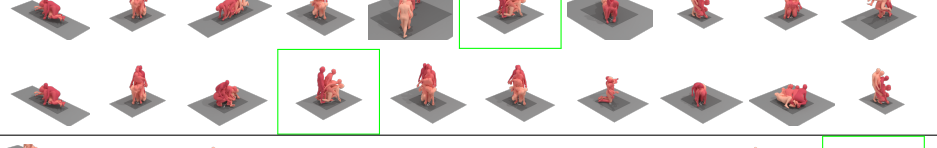
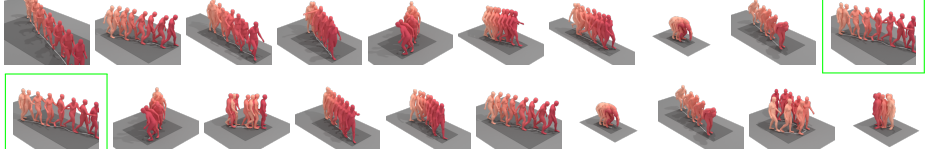
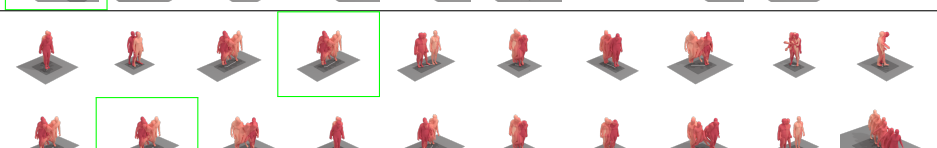
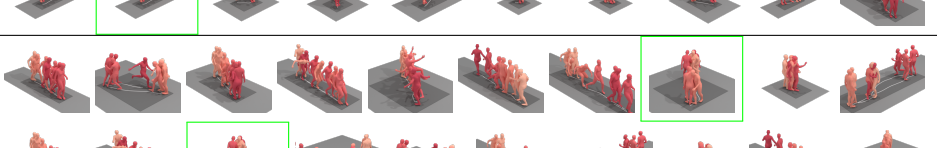
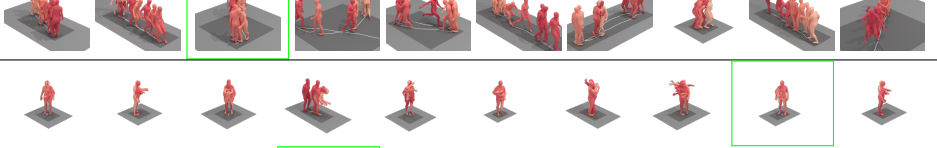
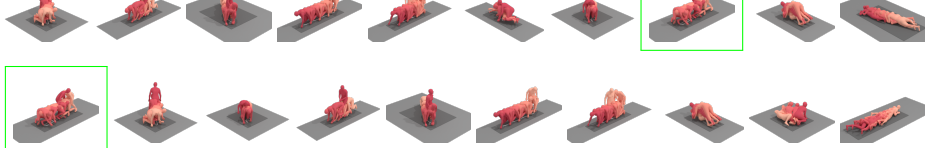
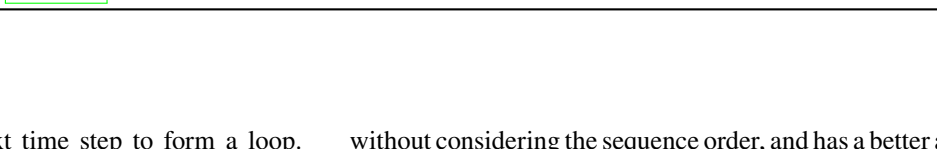
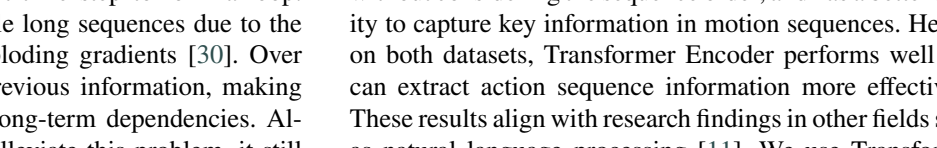
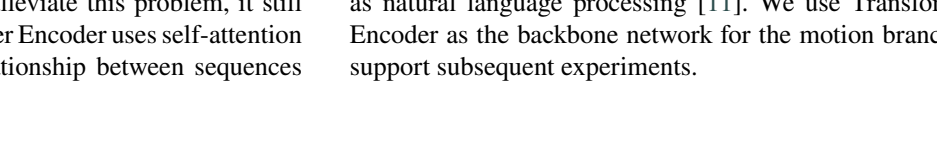
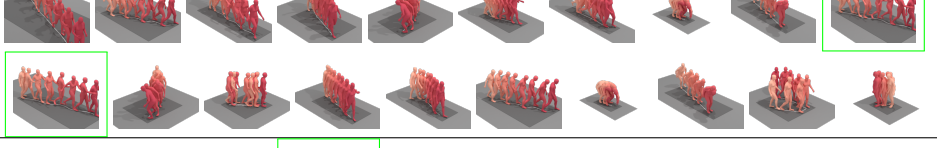
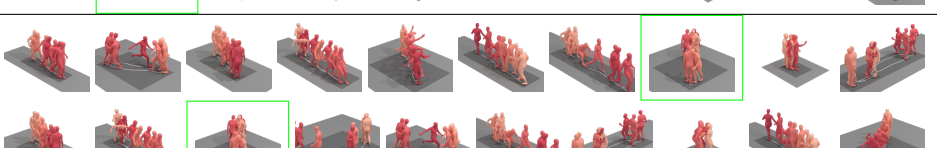
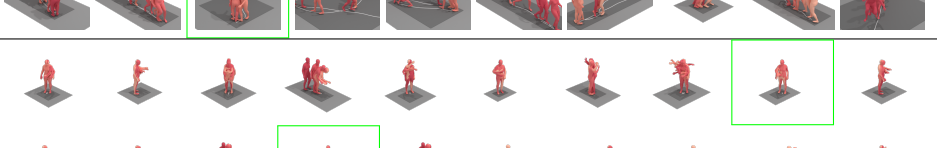
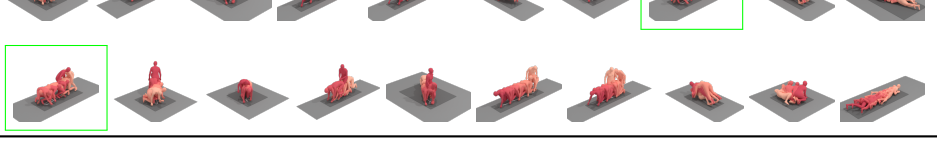
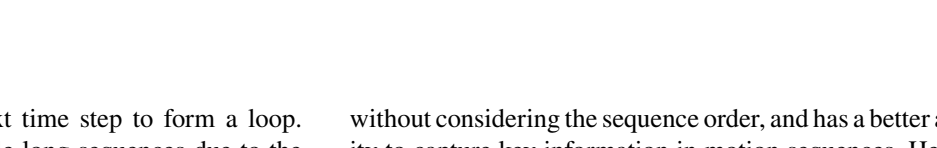
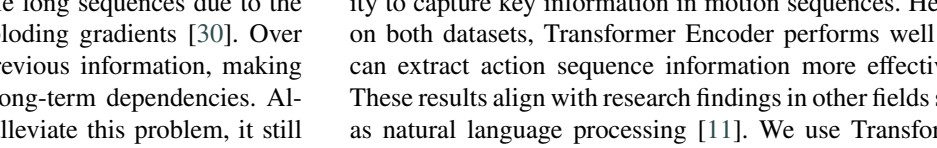
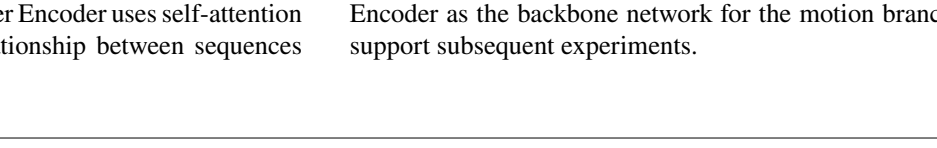
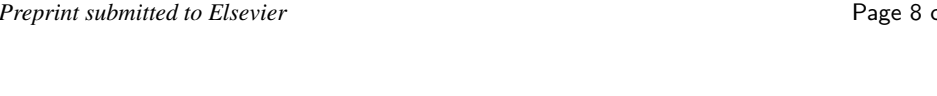
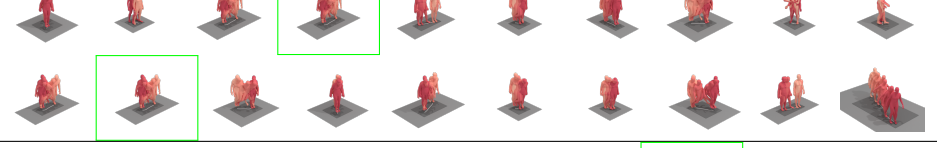
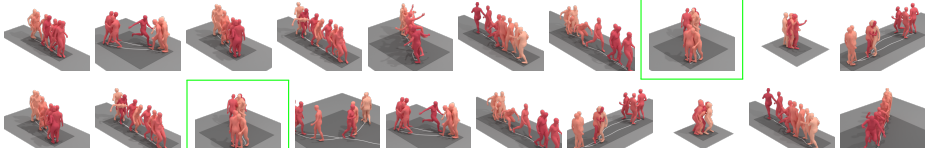
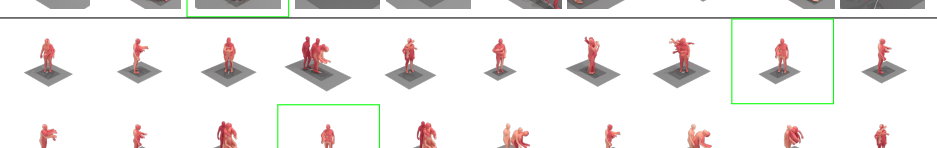
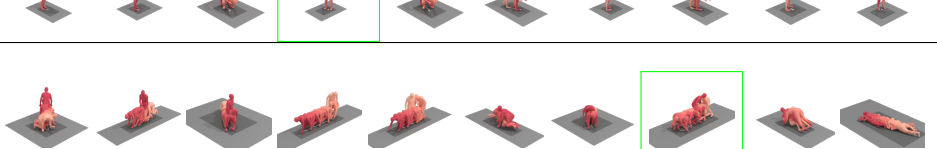
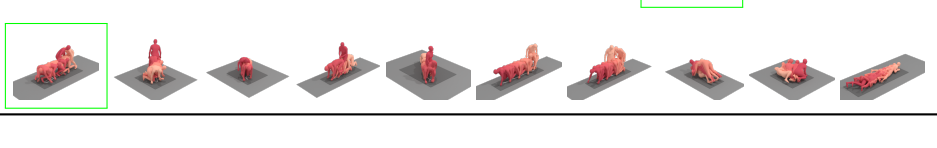
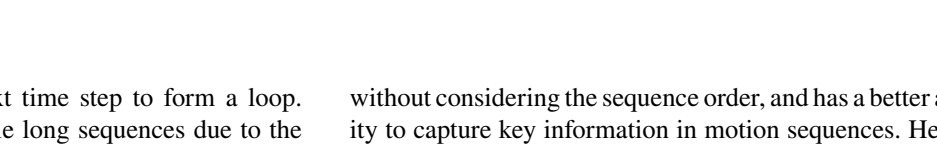
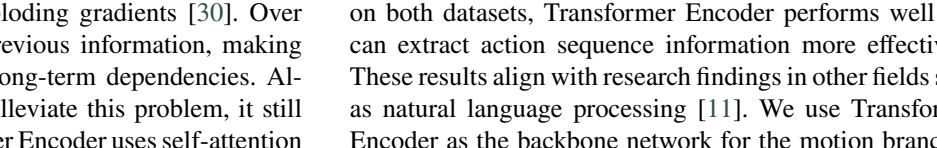
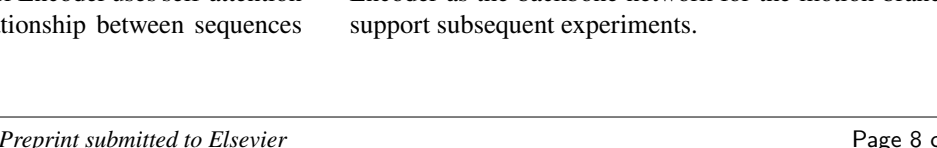
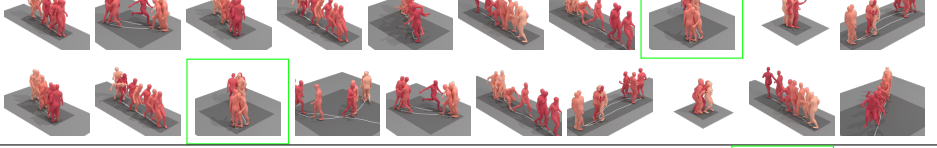
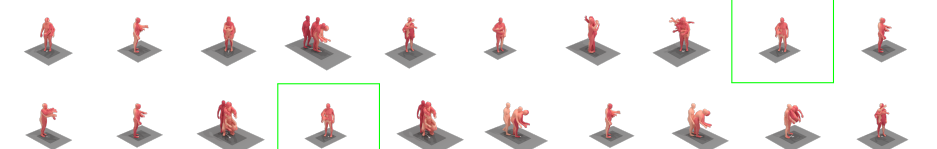
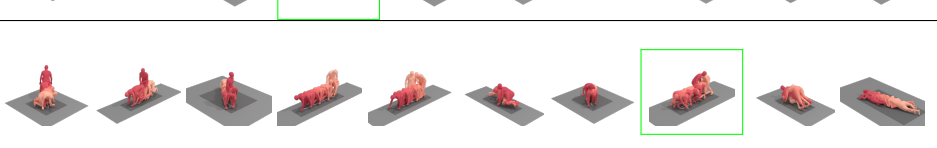
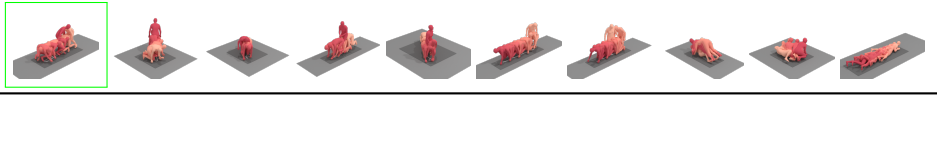
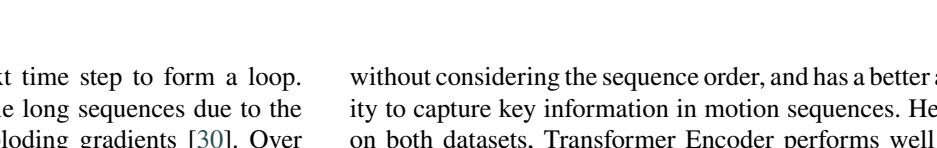
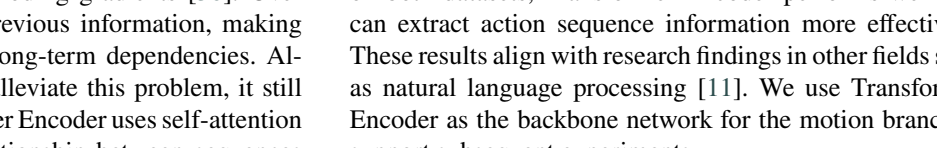
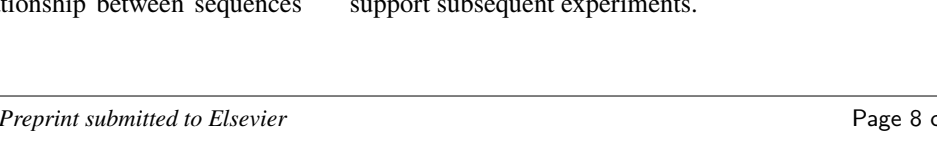
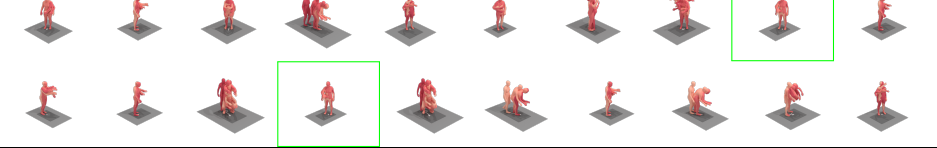
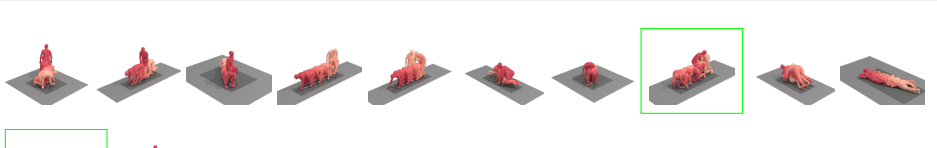
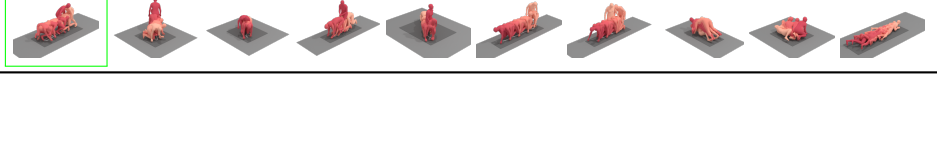
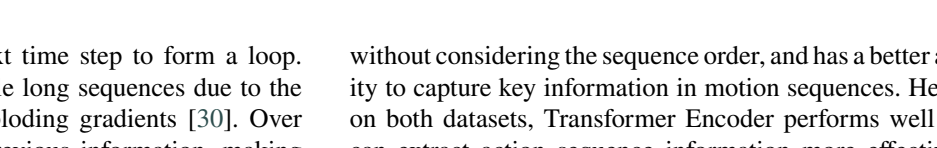
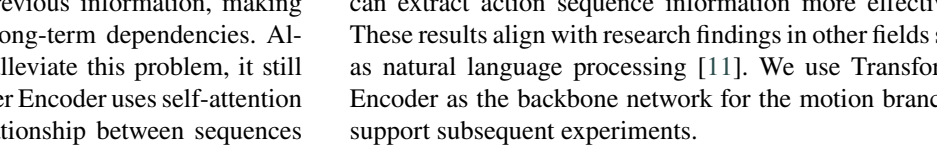
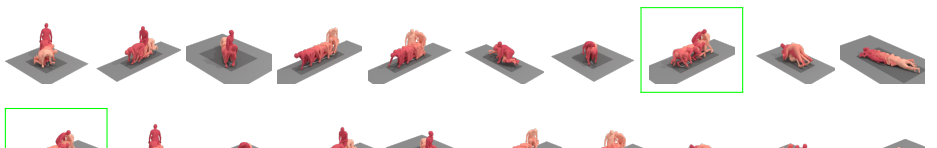
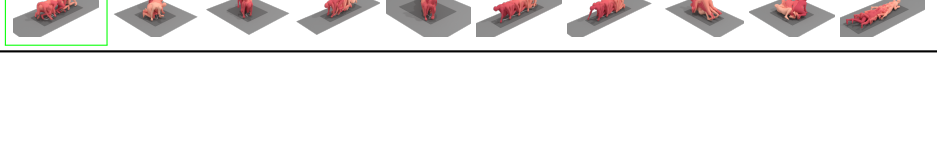
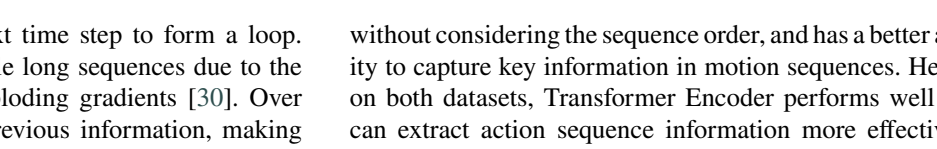
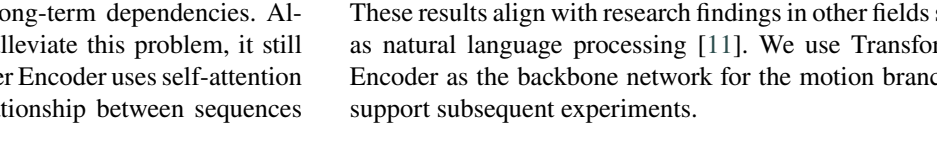
## 4.3. Comparison with RNN-type neural networks

We conducted contrast experiments to evaluate the performance of several commonly used neural network architectures, including RNN, GRU, LSTM, and Transformer Encoder, as the motion encoder backbone network. The R-sum scores obtained by different neural network layer models were demonstrated in Figure 4a. Additionally, Figure 4b shows the distribution of motion sequence lengths in two datasets (downsampled), revealing the presence of excessively long sequences in both datasets. Most of the motion lengths in HumanML3D were distributed between 161-200 frames, while 7.5% of the sequence lengths in KIT-ML exceeded 200 frames.

Our experimental results demonstrate that RNN-type neural networks perform slightly worse than Transformer Encoder on both datasets. One possible reason behind this observation is that the working principle of RNN-type neural networks combines the current input state with the previous state to calculate the output, and passes the current input and

**Table 1**

Motion retrieval results on HumanML3D. We visualize top 10 results for a given query. The images marked with a green box represent the ground-truth corresponding to the query.

Query	Top-10 Retrieved Motions									
<i>a person is sprinting fast.</i>										
<i>someone working out as the get up off the floor.</i>										
<i>a person walks forward while twisting their torso side to side.</i>										
<i>a figure takes one long side-step to the right over an object.</i>										
<i>the person took a leap forward and then turned around and took a leap pack.</i>										
<i>a person is performing a circular wiping motion.</i>										
<i>a person turns to the left and gets down on his hands and crawls forward, towards the left, then crawls back to the area he started and gets up.</i>										

◊ SH Loss

♡ Our MildTriple Loss

the previous output to the next time step to form a loop. This makes it difficult to handle long sequences due to the problem of vanishing and exploding gradients [30]. Over time, the model may forget previous information, making it unable to effectively learn long-term dependencies. Although LSTM and GRU can alleviate this problem, it still persists. In contrast, Transformer Encoder uses self-attention mechanisms to model the relationship between sequences

without considering the sequence order, and has a better ability to capture key information in motion sequences. Hence, on both datasets, Transformer Encoder performs well and can extract action sequence information more effectively. These results align with research findings in other fields such as natural language processing [11]. We use Transformer Encoder as the backbone network for the motion branch to support subsequent experiments.

**Table 2**

Results of ablation experiment on KIT-ML.

Method	KIT-ML									
	Motion Retrieval					Text Retrieval				
	R@1↑	R@5↑	R@10↑	Med R↓	R@1↑	R@5↑	R@10↑	Med R↓	R-sum↑	
SH Loss [33]	9.1	33.4	50.3	10.0	9.4	33.1	48.0	12.0	183.0	
MH Loss [14]	10.6	33.9	50.7	10.0	11.2	32.3	43.4	15.0	182.1	
Our MildTriple Loss	9.7	34.5	52.4	10.0	11.0	30.7	47.8	12.0	186.1	
<b>Our MildTriple Loss (fine-tune)</b>	<b>12.2</b>	<b>41.7</b>	<b>59.1</b>	<b>8.0</b>	<b>13.9</b>	<b>41.0</b>	<b>55.0</b>	<b>8.0</b>	<b>222.8</b>	

**Table 3**

Results of ablation experiment on HumanML3D.

Method	HumanML3D									
	Motion Retrieval					Text Retrieval				
	R@1↑	R@5↑	R@10↑	Med R↓	R@1↑	R@5↑	R@10↑	Med R↓	R-sum↑	
SH Loss [33]	10.9	34.4	48.1	11.0	13.2	41.5	56.5	8.0	204.6	
MH Loss [14]	10.7	35.1	48.9	11.0	14.0	43.3	58.1	7.0	210.1	
Our MildTriple Loss	13.3	38.9	52.9	9.0	16.1	45.9	60.5	6.0	227.7	
<b>Our MildTriple Loss (fine-tune)</b>	<b>17.3</b>	<b>48.9</b>	<b>62.9</b>	<b>6.0</b>	<b>21.1</b>	<b>54.7</b>	<b>71.5</b>	<b>5.0</b>	<b>276.4</b>	

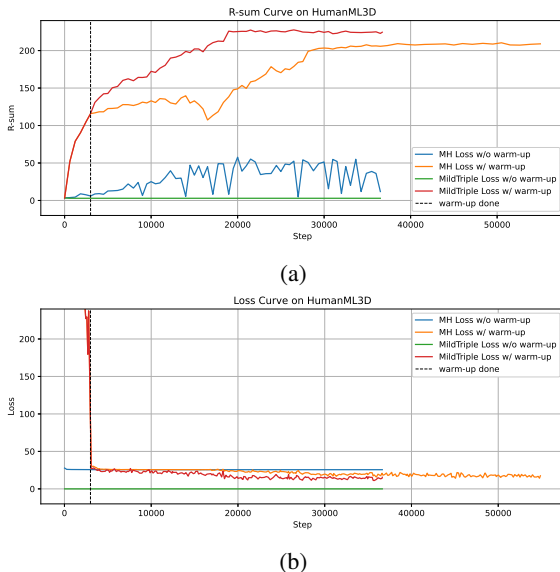


**Figure 5:** Figure (a) illustrates the R-sum scores during warm-up and no warm-up conditions using both MH loss and MildTriple loss on HumanML3D dataset. Figure (b) presents the variation in loss under the same circumstances.

#### 4.4. Ablation Studies

##### 4.4.1. Ablation of Soft-Hard Negative Mining

We used the model trained with the SH loss function as our baseline and ablated the usage of hard negative mining (MH Loss) and soft-hard negative mining (MildTriple Loss) methods to evaluate their contributions to the final results. The results evaluated on two datasets are presented in Table 2 and Table 3. Notably, we utilized the SH Loss for warm-up for the ablation methods, which allowed our model to quickly differentiate between the diverse data and converge the loss. In Section 4.4.2, we have discussed the necessity of warm-up.

From the table, the MildTriple Loss method outperformed SH Loss and MH Loss on both HumanML3D and KIT-ML datasets. On the HumanML3D dataset, the MildTriple Loss improved the R@1, R@5, and R@10 metrics (sum of motion and text retrieval results) by 5.3%, 9.9%, and 8.8%, respectively, compared to SH Loss. Additionally, the Med R was reduced by 2.0, while the R-sum was increased by 23.1 points. On the KIT-ML dataset, the MildTriple Loss also improved the R-sum metric by 3.1 points compared to SH Loss, and the Med R metric was reduced by 2.0. The previous hard negative mining strategy did not achieve the expected effect because it optimized too many false negative samples, especially on KIT-ML where R-sum decreased relative to SH Loss. Our MildTriple Loss, which adopts the idea of soft-hard negative mining, can avoid unnecessary semantic conflicts caused by false negatives and improve the model performance. More intuitively, we have visualized the comparison of its retrieval results with SH Loss in Tables 1 and 4.

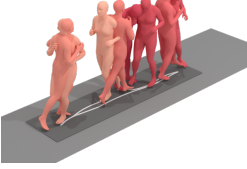
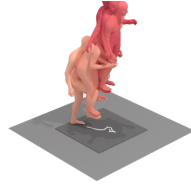
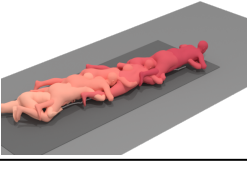
Finally, based on the MildTriple Loss method, we fine-tuned the text branch backbone network (i.e., DistilBERT). All metrics of the MildTriple Loss method after fine-tuning reached their highest values. Particularly, the R@5 and R@10 metrics for motion retrieval on the HumanML3D dataset increased by 10.0%, and the R-sum reached 276.4 points. The Med R also further reduced after fine-tuning, with motion retrieval and text retrieval on HumanML3D reduced to 6.0 and 5.0, respectively, and motion retrieval and text retrieval on KIT-ML reduced to 8.0.

##### 4.4.2. Ablation of Warm-up

We observed that during training, direct use of the MH loss requires a long warm-up period, while direct use of the MildTriple loss does not improve the R-sum score throughout the process. To address this issue, we used the SH loss function for warm-up at the start of training and switched to

**Table 4**

Text retrieval results on HumanML3D. We visualize top 5 results of a given query. The ground-truth is highlighted in blue.

Query	Top-5 Retrieved Texts
	<ol style="list-style-type: none"> <li>1. the person is jogging back-and-forth to the left and right.</li> <li>2. a person jogs back and forth.</li> <li>3. a person jogs back and forth.</li> <li><b>4. person is jogging from left to right and then back to the center.</b></li> <li>5. a person ran in left and after right direction and returned.</li> </ol> <ol style="list-style-type: none"> <li>1. the person is jogging back-and-forth to the left and right.</li> <li><b>2. a person starts in the middle, runs to the right, then to the left, then returns back to their starting position.</b></li> <li>3. person is jogging from left to right and then back to the center.</li> <li>4. a person jogs back and forth.</li> <li>5. a person jogs back and forth.</li> </ol>
	<ol style="list-style-type: none"> <li>1. the person is climbing on a stepstool to change a lightbulb.</li> <li>2. a person holds onto something while walking up and down stairs.</li> <li>3. a person takes a step to the right side and up onto a ladder to change a lightbulb.</li> <li>4. someone climbs a step, walks and descends a step.</li> <li><b>5. a person climbs up a ladder.</b></li> </ol> <ol style="list-style-type: none"> <li>1. the person climbs up something for few steps.</li> <li><b>2. a person climbs up a ladder.</b></li> <li><b>3. the person is climbing up to reach some thing.</b></li> <li>4. a person hesitantly climbs a ladder.</li> <li>5. the person is climbing on a stepstool to change a lightbulb.</li> </ol>
	<ol style="list-style-type: none"> <li>1. a person walks on a treadmill at a slow pace.</li> <li>2. a person is walking in place at a slow pace.</li> <li>3. the man is slowly walking on the treadmill.</li> <li><b>4. the person is walking on a treadmill slowly.</b></li> <li>5. a person walking slowly on a treadmill.</li> </ol> <ol style="list-style-type: none"> <li><b>1. the person is walking on a treadmill slowly.</b></li> <li>2. a person walks on a treadmill at a slow pace.</li> <li>3. the man is slowly walking on the treadmill.</li> <li>4. a person walking slowly on a treadmill.</li> <li>5. a person is walking in place at a slow pace.</li> </ol>
	<ol style="list-style-type: none"> <li>1. walking while swinging both arms from left to right.</li> <li>2. a person is dancing with left hand holding someone.</li> <li>3. holding a partner, a person dances a waltz.</li> <li>4. a person strums a guitar/banjo with their right hand while holding the neck in their left.</li> <li><b>5. a person is doing the cha cha dance.</b></li> </ol> <ol style="list-style-type: none"> <li><b>1. a person performs the waltz.</b></li> <li>2. holding a partner, a person dances a waltz.</li> <li>3. a person is dancing with left hand holding someone.</li> <li>4. a figure waltzes, taking large steps in a circle rhythmically.</li> <li>5. a person is dancing the cha cha.</li> </ol>
	<ol style="list-style-type: none"> <li>1. the person is crawling in their hands and knees.</li> <li>2. a person drops down to their hands and knees and proceeds to crawl forward.</li> <li><b>3. a man crawls forward on his stomach.</b></li> <li>4. laying down on face and crawling backwards.</li> <li>5. a man gets on his hands and knees and crawls forward.</li> </ol> <ol style="list-style-type: none"> <li><b>1. a man crawls forward on his stomach.</b></li> <li><b>2. this person crawls on all fours with belly close to the ground.</b></li> <li>3. a person crawls along the ground on their belly.</li> <li>4. the person is crawling in their hands and knees.</li> <li>5. laying down on face and crawling backwards.</li> </ol>

SH Loss

Our MildTriple Loss

the MH or MildTriple loss function for the rest of the training after several epochs. Figure 5 depicts the R-sum score and the loss variation w/ and w/o warm-up on HumanML3D, which shows that the R-sum score steadily increases and the loss decreases after warm-up. To explain why direct use of the MildTriple loss results in zero loss and no change in R-sum, we visualized the similarity matrices under different training batches, as shown in Figure 6. At the beginning of training (at epoch 1), the matrices in Figure 6a and 6d are mostly red, which means that the similarities between the samples are roughly the same and highly similar, i.e., the model cannot distinguish differences between different samples. If the MildTriple loss is used directly for training, it will result in the negative sample set  $\mathcal{Y}_{MT}$  not being truly negative and therefore reducing the number of optimizable objects. In extreme cases, when  $\delta$  is set too small,  $\mathcal{Y}_{MT}$  will

include all negative samples, resulting in zero optimizable objects and a loss of zero as shown in Figure 5a. Therefore, we need to use the soft negative sample mining strategy only after the model has basic discriminability among samples within each modality, such as when the similarities between the samples are distinguishable. In other words, we start using MildTriple loss after training the model to be relatively stable with the SH loss, e.g., at epoch-6 or epoch-11.

#### 4.5. Influence of the threshold $\delta$

We changed the thresholds  $\delta_{hetero}$  and  $\delta_{homo}$  to evaluate their impact on Eq. 6. Table 5 illustrates the R-sum results obtained using different thresholds on HumanML3D and KIT-ML. By observing the fluctuations in R-sum, we found that when  $\delta_{homo}$  and  $\delta_{hetero}$  are relatively small, the results obtained are either close to or even lower than MH Loss

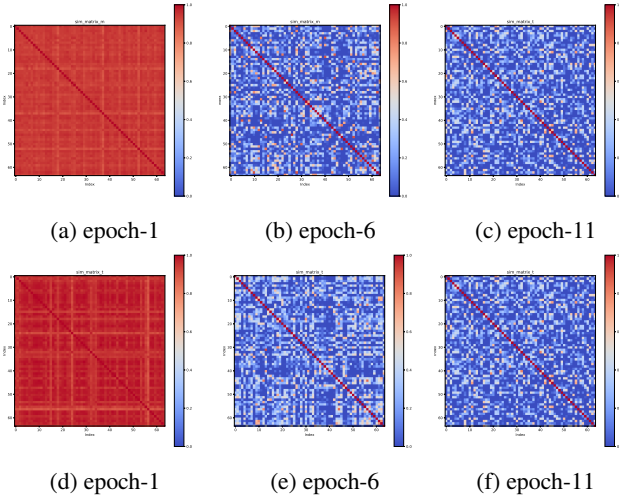


**Figure 6:** Snapshot of the similarity matrix among the samples of a training mini-batch in different epochs on HumanML3D. The first and second rows respectively display the similarity matrices within the motion and text modalities, in which the colors vary from blue to red represent the similarity between samples from weak to strong.

(when  $\delta_{homo}$  and  $\delta_{hetero}$  equal 1.0). For example, when  $\delta_{hetero}$  and  $\delta_{homo}$  are both 0.6, the R-sum is only 2.6 higher than MH Loss on HumanML3D and even 6.8 lower on KIT-ML. This indicates that when the threshold is less than a certain level, the MildTriple Loss may mistakenly label some normal negative samples as hard negative samples, which resemble the anchor sample only slightly but do not share the same semantic meaning as the anchor. Protecting these normal negative samples leads to a decline in the ability of MildTriple Loss to select soft-hard negative samples, thus affecting the overall performance of our model.

#### 4.6. Limitations

Our model has several limitations. First, there is an uneven allocation of action clusters in the dataset we used. We extracted verb-based "action phrases" from each sentence in the HumanML3D dataset, such as "run around" for the sentence "a person is running around," by detecting and morphing verbs and adding complements. We used this process to group sequences with the same action phrases and obtained a total of 25,661 distinct action clusters, with a highly unbalanced distribution. "Walk" appeared the most, a total of 1,531 times, while 24,864 actions appeared less than 10 times, accounting for about 96.8%. Only 22,626 actions appeared once, which accounts for about 89%. Due to the uneven distribution of actions, some samples with extremely low occurrence frequencies, such as "fishing" and "karate," are difficult to retrieve during testing due to even minor dissimilarities in feature space, despite a certain level of similarity. Secondly, the high frequency of appearance of some actions and the overly generic nature of some text descriptions result in a large number of false negatives in the retrieved results. For example, for the query "A person walks backwards", there are minor differences between the

**Table 5**

Experimental results with different  $\delta_{hetero}$  and  $\delta_{homo}$  values on HumanML3D and KIT-ML datasets.

		R-sum	
		HumanML3D	KIT-ML
(A)	0.6	215.2	180.1
	0.7	221.1	183.5
	0.8	221.6	192.0
	0.9	220.1	<b>193.0</b>
	1.0	218.4	<b>193.0</b>
(B)	0.6	218.2	183.0
	0.7	221.6	189.9
	0.8	220.6	187.8
	0.9	<b>222.2</b>	183.6
	1.0	219.1	189.7
(C)	0.6	217.8	188.1
	0.7	220.4	189.1
	0.8	220.1	186.2
	0.9	216.7	183.4
	1.0	219.9	185.6
(D)	0.6	218.6	189.9
	0.7	221.2	189.4
	0.8	220.7	183.1
	0.9	217.4	183.5
	1.0	216.0	187.7
(E)	0.6	220.3	188.3
	0.7	216.8	189.4
	0.8	217.3	186.4
	0.9	218.2	185.5
	1.0	212.6	186.9

retrieved motions that rank higher than the ground truth (e.g., inconsistent steps or incomplete displacement), which can reflect the semantics of the query, but they cannot be considered as correct retrieval answers. This is one of the reasons for the low R@1 scores in our experiment results. Lastly, due to the difference in human body scales and movement ranges in different datasets, our motion branch lacks pre-trained models with outstanding feature extraction ability and generalization ability, such as those in the visual field like VGG19 and ResNet50 [23]. Therefore, we have to train our motion encoder from scratch, which easily leads to overfitting because the model lacks general representation ability for other data.

## 5. Conclusion

In this work, we propose a 3D human motion and text retrieval model consisting of simple yet powerful motion and text encoders used to learn representations from two different modalities. Our approach is a meaningful attempt to accurately match 3D human motion with natural language descriptions, with broad practical applications. Furthermore, we propose the MildTriple Loss, a loss function featuring soft margin negative sample mining, to reduce semantic conflicts caused by false negatives. We evaluate

our model on the latest HumanML3D and KIT-ML datasets, and demonstrate the effectiveness of our proposed method, achieving promising results. In future work, we aim to explore the possibility of extending the MildTriple Loss to other retrieval tasks and generalize our loss function to other domains by adjusting the threshold. Moreover, we will strive to leverage the interaction between multiple modalities to improve retrieval recall, such as recent methods that fuse multi-modal information into one encoder [34, 53].

## CRediT authorship contribution statement

**Sheng Yan:** Conceptualization, Methodology, Software, Investigation, Writing - Original Draft. **Haoqiang Wang:** Data Curation, Validation, Formal analysis. **Xin Du:** Methodology, Software, Visualization. **Mengyuan Liu:** Conceptualization, Methodology, Supervision, Project administration. **Hong Liu:** Conceptualization, Supervision.

## References

- [1] Ahn, H., Ha, T., Choi, Y., Yoo, H., Oh, S., 2018. Text2action: Generative adversarial synthesis from language to action, in: IEEE International Conference on Robotics and Automation (ICRA), pp. 5915–5920.
- [2] Ahuja, C., Morency, L.P., 2019. Language2pose: Natural language grounded pose forecasting, in: International Conference on 3D Vision (3DV), pp. 719–728.
- [3] Bain, M., Nagrani, A., Varol, G., Zisserman, A., 2021. Frozen in time: A joint video and image encoder for end-to-end retrieval, in: IEEE International Conference on Computer Vision (ICCV), pp. 1728–1738.
- [4] Cao, D., Chu, J., Zhu, N., Nie, L., 2020. Cross-modal recipe retrieval via parallel-and cross-attention networks learning. Knowledge-Based Systems 193, 105428.
- [5] Chen, J., Zhang, L., Wang, Q., Bai, C., Kpalma, K., 2022. Intra-modal constraint loss for image-text retrieval, in: IEEE International Conference on Image Processing (ICIP), pp. 4023–4027.
- [6] Chen, T., Kornblith, S., Norouzi, M., Hinton, G., 2020a. A simple framework for contrastive learning of visual representations, in: International Conference on Machine Learning (ICML), pp. 1597–1607.
- [7] Chen, X., Fan, H., Girshick, R., He, K., 2020b. Improved baselines with momentum contrastive learning. arXiv:2003.04297 .
- [8] Colla, D., Mensa, E., Radicioni, D.P., 2020. Novel metrics for computing semantic similarity with sense embeddings. Knowledge-Based Systems 206, 106346.
- [9] Cui, W., Bai, L., Yang, X., Liang, J., 2023. A new contrastive learning framework for reducing the effect of hard negatives. Knowledge-Based Systems 260, 110121.
- [10] Delmas, G., Weinzaepfel, P., Lucas, T., Moreno-Noguer, F., Rogez, G., 2022. Posescript: 3d human poses from natural language, in: European Conference on Computer Vision (ECCV), pp. 346–362.
- [11] Devlin, J., Chang, M.W., Lee, K., Toutanova, K., 2018. Bert: Pre-training of deep bidirectional transformers for language understanding. arXiv:1810.04805 .
- [12] Dong, X., Zhang, H., Dong, X., Lu, X., 2021. Iterative graph attention memory network for cross-modal retrieval. Knowledge-Based Systems 226, 107138.
- [13] Dosovitskiy, A., Beyer, L., Kolesnikov, A., Weissenborn, D., Zhai, X., Unterthiner, T., Dehghani, M., Minderer, M., Heigold, G., Gelly, S., et al., 2020. An image is worth 16x16 words: Transformers for image recognition at scale. arXiv:2010.11929 .
- [14] Faghri, F., Fleet, D.J., Kiros, J.R., Fidler, S., 2017. Vse++: Improving visual-semantic embeddings with hard negatives. arXiv:1707.05612 .
- [15] Gabeur, V., Sun, C., Alahari, K., Schmid, C., 2020. Multi-modal transformer for video retrieval, in: European Conference on Computer Vision (ECCV), pp. 214–229.
- [16] Ghosh, P., Song, J., Aksan, E., Hilliges, O., 2017. Learning human motion models for long-term predictions, in: International Conference on 3D Vision (3DV), pp. 458–466.
- [17] Gong, Y., Cosma, G., Fang, H., 2021. On the limitations of visual-semantic embedding networks for image-to-text information retrieval. Journal of Imaging 7, 125.
- [18] Guo, C., Zou, S., Zuo, X., Wang, S., Ji, W., Li, X., Cheng, L., 2022. Generating diverse and natural 3d human motions from text, in: IEEE Conference on Computer Vision and Pattern Recognition (CVPR), pp. 5152–5161.
- [19] Guo, C., Zuo, X., Wang, S., Zou, S., Sun, Q., Deng, A., Gong, M., Cheng, L., 2020. Action2motion: Conditioned generation of 3d human motions, in: ACM International Conference on Multimedia (ACM MM), pp. 2021–2029.
- [20] Hadsell, R., Chopra, S., LeCun, Y., 2006. Dimensionality reduction by learning an invariant mapping, in: IEEE Conference on Computer Vision and Pattern Recognition (CVPR), pp. 1735–1742.
- [21] Hafner, F.M., Bhuiyan, A., Kooij, J.F., Granger, E., 2019. Rgb-depth cross-modal person re-identification, in: IEEE International Conference on Advanced Video and Signal Based Surveillance (AVSS), pp. 1–8.
- [22] He, K., Fan, H., Wu, Y., Xie, S., Girshick, R., 2020. Momentum contrast for unsupervised visual representation learning, in: IEEE/CVF Conference on Computer Vision and Pattern Recognition (CVPR), pp. 9729–9738.
- [23] He, K., Zhang, X., Ren, S., Sun, J., 2016. Deep residual learning for image recognition, in: IEEE Conference on Computer Vision and Pattern Recognition (CVPR), pp. 770–778.
- [24] Ho, J., Salimans, T., Gritsenko, A., Chan, W., Norouzi, M., Fleet, D.J., 2022. Video diffusion models. arXiv:2204.03458 .
- [25] Hodosh, M., Young, P., Hockenmaier, J., 2013. Framing image description as a ranking task: Data, models and evaluation metrics. Journal of Artificial Intelligence Research 47, 853–899.
- [26] Holden, D., Saito, J., Komura, T., 2016. A deep learning framework for character motion synthesis and editing. ACM Transactions on Graphics 35, 1–11.
- [27] Huang, Q., Jansen, A., Lee, J., Ganti, R., Li, J.Y., Ellis, D.P., 2022. Mulan: A joint embedding of music audio and natural language. arXiv:2208.12415 .
- [28] Jia, C., Yang, Y., Xia, Y., Chen, Y.T., Parekh, Z., Pham, H., Le, Q., Sung, Y.H., Li, Z., Duerig, T., 2021. Scaling up visual and vision-language representation learning with noisy text supervision, in: International Conference on Machine Learning (ICML), pp. 4904–4916.
- [29] Jin, M., Zhang, H., Zhu, L., Sun, J., Liu, L., 2022. Coarse-to-fine dual-level attention for video-text cross modal retrieval. Knowledge-Based Systems 242, 108354.
- [30] Jozefowicz, R., Zaremba, W., Sutskever, I., 2015. An empirical exploration of recurrent network architectures, in: International Conference on Machine Learning (ICML), pp. 2342–2350.
- [31] Karpathy, A., Fei-Fei, L., 2015. Deep visual-semantic alignments for generating image descriptions, in: IEEE Conference on Computer Vision and Pattern Recognition (CVPR), pp. 3128–3137.
- [32] Kingma, D.P., Ba, J., 2014. Adam: A method for stochastic optimization. arXiv:1412.6980 .
- [33] Kiros, R., Salakhutdinov, R., Zemel, R.S., 2014. Unifying visual-semantic embeddings with multimodal neural language models. arXiv:1411.2539 .
- [34] Li, J., Selvaraju, R., Gotmare, A., Joty, S., Xiong, C., Hoi, S.C.H., 2021. Align before fuse: Vision and language representation learning with momentum distillation. Advances in Neural Information Processing Systems (NeurIPS) 34, 9694–9705.
- [35] Li, S., Xiao, T., Li, H., Yang, W., Wang, X., 2017a. Identity-aware textual-visual matching with latent co-attention, in: IEEE International Conference on Computer Vision (ICCV), pp. 1890–1899.

[36] Li, Z., Zhou, Y., Xiao, S., He, C., Huang, Z., Li, H., 2017b. Auto-conditioned recurrent networks for extended complex human motion synthesis. *arXiv:1707.05363*.

[37] Liu, M., Liu, H., Chen, C., 2017. Enhanced skeleton visualization for view invariant human action recognition. *Pattern Recognition* 68, 346–362.

[38] Liu, M., Meng, F., Chen, C., Wu, S., 2023. Novel motion patterns matter for practical skeleton-based action recognition, in: AAAI Conference on Artificial Intelligence (AAAI).

[39] Liu, M., Meng, F., Liang, Y., 2022a. Generalized pose decoupled network for unsupervised 3d skeleton sequence-based action representation learning. *Cyborg and Bionic Systems* 2022, 0002.

[40] Liu, Y., Liu, H., Wang, H., Liu, M., 2022b. Regularizing visual semantic embedding with contrastive learning for image-text matching. *IEEE Signal Processing Letters* 29, 1332–1336.

[41] Long, X., Zhang, Z., Li, Y., 2022. Multi-network contrastive learning of visual representations. *Knowledge-Based Systems* 258, 109991.

[42] Loper, M., Mahmood, N., Romero, J., Pons-Moll, G., Black, M.J., 2015. Smpl: A skinned multi-person linear model. *ACM transactions on graphics* 34, 1–16.

[43] Lu, J., Batra, D., Parikh, D., Lee, S., 2019. Vilbert: Pretraining task-agnostic visiolinguistic representations for vision-and-language tasks. *Advances in Neural Information Processing Systems (NeurIPS) 32*.

[44] Mahmood, N., Ghorbani, N., Troje, N.F., Pons-Moll, G., Black, M.J., 2019. Amass: Archive of motion capture as surface shapes, in: IEEE International Conference on Computer Vision (ICCV), pp. 5442–5451.

[45] Martinez, J., Black, M.J., Romero, J., 2017. On human motion prediction using recurrent neural networks, in: IEEE Conference on Computer Vision and Pattern Recognition (CVPR), pp. 2891–2900.

[46] Petrovich, M., Black, M.J., Varol, G., 2022. Temos: Generating diverse human motions from textual descriptions, in: European Conference on Computer Vision (ECCV).

[47] Plappert, M., Mandery, C., Asfour, T., 2016. The kit motion-language dataset. *Big data* 4, 236–252.

[48] Plappert, M., Mandery, C., Asfour, T., 2018. Learning a bidirectional mapping between human whole-body motion and natural language using deep recurrent neural networks. *Robotics and Autonomous Systems* 109, 13–26.

[49] Radford, A., Kim, J.W., Hallacy, C., Ramesh, A., Goh, G., Agarwal, S., Sastry, G., Askell, A., Mishkin, P., Clark, J., et al., 2021. Learning transferable visual models from natural language supervision, in: International Conference on Machine Learning (ICML), pp. 8748–8763.

[50] Ramesh, A., Dhariwal, P., Nichol, A., Chu, C., Chen, M., 2022. Hierarchical text-conditional image generation with clip latents. *arXiv:2204.06125*.

[51] Sanh, V., Debut, L., Chaumond, J., Wolf, T., 2019. Distilbert, a distilled version of bert: smaller, faster, cheaper and lighter. *arXiv:1910.01108*.

[52] Sun, C., Myers, A., Vondrick, C., Murphy, K., Schmid, C., 2019. Videobert: A joint model for video and language representation learning, in: IEEE/CVF International Conference on Computer Vision (ICCV), pp. 7464–7473.

[53] Tan, H., Bansal, M., 2019. Lxmert: Learning cross-modality encoder representations from transformers. *arXiv:1908.07490*.

[54] Tevet, G., Raab, S., Gordon, B., Shafir, Y., Cohen-Or, D., Bermano, A.H., 2022. Human motion diffusion model. *arXiv:2209.14916*.

[55] Tian, Y., Sun, C., Poole, B., Krishnan, D., Schmid, C., Isola, P., 2020. What makes for good views for contrastive learning? *Advances in Neural Information Processing Systems (NeurIPS) 33*, 6827–6839.

[56] Tu, Z., Li, H., Zhang, D., Dauwels, J., Li, B., Yuan, J., 2019. Action-stage emphasized spatiotemporal vlad for video action recognition. *IEEE Transactions on Image Processing* 28, 2799–2812.

[57] Vaswani, A., Shazeer, N., Parmar, N., Uszkoreit, J., Jones, L., Gomez, A.N., Kaiser, Ł., Polosukhin, I., 2017. Attention is all you need 30.

[58] Wang, J., Song, Y., Leung, T., Rosenberg, C., Wang, J., Philbin, J., Chen, B., Wu, Y., 2014. Learning fine-grained image similarity with deep ranking, in: IEEE Conference on Computer Vision and Pattern Recognition (CVPR), pp. 1386–1393.

[59] Wang, L., Li, Y., Lazebnik, S., 2016. Learning deep structure-preserving image-text embeddings, in: IEEE Conference on Computer Vision and Pattern Recognition (CVPR), pp. 5005–5013.

[60] Wang, Z., Xu, X., Wei, J., Xie, N., Shao, J., Yang, Y., 2023. Quaternion representation learning for cross-modal matching. *Knowledge-Based Systems* , 110505.

[61] Yamada, T., Matsunaga, H., Ogata, T., 2018. Paired recurrent autoencoders for bidirectional translation between robot actions and linguistic descriptions. *IEEE Robotics and Automation Letters* 3, 3441–3448.

[62] Yang, C., Zou, J., Wu, J., Xu, H., Fan, S., 2022. Supervised contrastive learning for recommendation. *Knowledge-Based Systems* 258, 109973.

[63] Yu, J., Zhang, W., Yang, Z., Qin, Z., Hu, Y., 2020. Cross-modal learning with prior visual relation knowledge. *Knowledge-Based Systems* 203, 106150.

[64] Yuan, X., Lin, Z., Kuen, J., Zhang, J., Wang, Y., Maire, M., Kale, A., Faieta, B., 2021. Multimodal contrastive training for visual representation learning, in: IEEE/CVF Conference on Computer Vision and Pattern Recognition (CVPR), pp. 6995–7004.

[65] Zhang, J., Jia, Y., Xie, W., Tu, Z., 2022a. Zoom transformer for skeleton-based group activity recognition. *IEEE Transactions on Circuits and Systems for Video Technology* 32, 8646–8659.

[66] Zhang, L., Wu, H., Chen, Q., Deng, Y., Siebert, J., Li, Z., Han, Y., Kong, D., Cao, Z., 2022b. Vldeformer: Vision–language decomposed transformer for fast cross-modal retrieval. *Knowledge-Based Systems* 252, 109316.

[67] Zhao, G., Zhang, C., Shang, H., Wang, Y., Zhu, L., Qian, X., 2023. Generative label fused network for image-text matching. *Knowledge-Based Systems* , 110280.

[68] Zhou, F., Dai, Y., Gao, Q., Wang, P., Zhong, T., 2021. Self-supervised human mobility learning for next location prediction and trajectory classification. *Knowledge-Based Systems* 228, 107214.

[69] Zhou, Y., Barnes, C., Lu, J., Yang, J., Li, H., 2019. On the continuity of rotation representations in neural networks, in: IEEE Conference on Computer Vision and Pattern Recognition (CVPR), pp. 5745–5753.

[70] Zolfaghari, M., Zhu, Y., Gehler, P., Brox, T., 2021. Crossclr: Cross-modal contrastive learning for multi-modal video representations, in: IEEE International Conference on Computer Vision (ICCV), pp. 1450–1459.

[71] Zou, X., Wu, S., Zhang, N., Bakker, E.M., 2022. Multi-label modality enhanced attention based self-supervised deep cross-modal hashing. *Knowledge-Based Systems* 239, 107927.